We are IntechOpen, the world's leading publisher of Open Access books
Built by scientists, for scientists

4,800
Open access books available

122,000
International authors and editors

135M
Downloads

Our authors are among the

154
Countries delivered to

TOP 1%
most cited scientists

12.2%
Contributors from top 500 universities

CLARIVATE ANALYTICS
BOOK CITATION INDEX
INDEXED

WEB OF SCIENCE™

Selection of our books indexed in the Book Citation Index in Web of Science™ Core Collection (BKCI)

Interested in publishing with us?
Contact book.department@intechopen.com

Numbers displayed above are based on latest data collected.
For more information visit www.intechopen.com

Chapter 7

The Properties and Application of Carbon Nanostructures

Petr Slepička, Tomáš Hubáček, Zdeňka Kolská, Simona Trostová, Nikola Slepičková Kasálková, Lucie Bačáková and Václav Švorčík

Additional information is available at the end of the chapter

http://dx.doi.org/10.5772/51062

1. Introduction

Nanocomposite carbon-based substrates are a large group of materials promising for medicine and various biotechnologies, particularly for coating biomaterials designed for hard tissue implantation, constructing biosensors and biostimulators or micropatterned surfaces for creation of cell microarrays for advanced genomics and proteomics. These substrates comprise nanocomposite hydrocarbon plasma polymer films, amorphous carbon, pyrolytic graphite, nanocrystalline diamond films, fullerene layers and carbon nanotube and nanoparticles-based substrates. Polymer/carbon composites have attracted increasing interest owing to their unique properties and numerous potential applications in the automotive, aerospace, construction and electronic industries.

Amorphous carbon, also referred to as diamond-like carbon (DLC), possesses a number of favourable properties, such as high hardness, a low friction coefficient, chemical inertness and high corrosion resistance, which is due to its particular structure, i.e. cohabitation of the sp^2 and sp^3 phases [1]. These properties make DLC attractive for coating bone and dental implants coating bone and dental implants in order to improve the resistance of these devices against wear, corrosion, debris formation and release of metallic ions, which can act as cytotoxic, immunogenic or even carcinogenic materials [2,3]. However, unmodified amorphous carbon usually acts as bioinert, i.e. not promoting its colonization with cells, which property prevents hemocoagulation, thrombosis and inflammatory reaction on the surfaces [4]. DLC coated materials have been utilized for construction of articular surfaces of joint prostheses [2] or blood-contacting devices (intravascular stents, mechanical heart valves, pumps).

From all nano-sized carbon allotropes, diamond has been often considered as the most advantageous material for advanced biomedical an biosensoric applications, which is

INTECH
open science | open minds

© 2013 Slepička et al., licensee InTech. This is an open access chapter distributed under the terms of the Creative Commons Attribution License (http://creativecommons.org/licenses/by/3.0), which permits unrestricted use, distribution, and reproduction in any medium, provided the original work is properly cited.

mainly due to the absence of its cytotoxicity, immunogenicity and other adverse reactions [5,6]. Other remarkable properties of nanodiamond, enabling its application in biotechnologies and medicine (particularly in hard tissue surgery), are high hardness, a low friction coefficient, and also high chemical, thermal and wear resistance. In our earlier studies and in studies by other authors, nanodiamond has proven itself as an excellent substrate for the adhesion, growth, metabolic activity and phenotypic maturation of several cell types in vitro, including osteogenic cells [5,7]. An interesting issue is doping of NCD films with boron. This doping renders the NCD films electroconductive [8]. Boron-doped NCD films have been applied in electronics and sensorics, e.g. for he construction of sensors for DNA hybridization [9], bacteria [10] or glucose [11].

Graphite is one of the most common allotropes of carbon, and the most stable form of carbon under standard conditions. However, despite its electrical conductivity, which is usually associated with the stimulatory effects on cell colonization and functioning, unmodified graphite is rather bioinert, i.e., less adhesive for cells [12]. It is due to a relatively low ability of graphite to adsorb cell adhesion-mediating proteins from the serum supplement of the culture medium [13] and also bone morphogenetic proteins (BMP), i.e. factors promoting the osteogenic cell differentiation [14]. Fullerenes are spheroidal molecules and are made exclusively of carbon atoms (e.g. C_{60}, C_{70}). Their unique hollow cage-like shape and structural analogy with clathrin-coated vesicles in cells support the idea of the potential use of fullerenes as drug or gene delivery agents [15]. Fullerenes display a diverse range of biological activity, which arises from their reactivity, due to the presence of double bonds and bending of sp^2 hybridized carbon atoms, which produces angle strain. Fullerenes can act either as acceptors or donors of electrons. When irradiated with ultraviolet or visible light, fullerenes can convert molecular oxygen into highly reactive singlet oxygen. Thus, they have the potential to inflict photodynamic damage on biological systems, including damage to cellular membranes, inhibition of various enzymes or DNA cleavage. This harmful effect can be exploited for photodynamic therapy of tumors [16], viruses including HIV-1 [17], broad spectrum of bacteria and fungi [18]. On the other hand, C_{60} is considered to be the world's most efficient radical scavenger. This is due to the relatively large number of conjugated double bonds in the fullerene molecule, which can be attacked by radical species. Thus, fullerenes would be suitable for applications in quenching oxygen radicals, and thus preventing inflammatory and allergic reactions [19] and damage of various tissues and organs, including blood vessels [20] and brain [21]. Finally, carbon nanotubes are formed by a single cylindrically-shaped graphene sheet (single-wall carbon nanotubes, referred usually to as SWNT or SWCNT) or several graphene sheets arranged concentrically (multi-wall carbon nanotubes, referred to as MWNT or MWCNT). Carbon nanotubes have excellent mechanical properties, mainly due to sp^2 bonds. The tensile strength of single-walled nanotubes is about one hundred times higher than that of the steel, while their specific weight is about six times lower [22]. Thus, carbon nanotubes could be utilized in hard tissue surgery, e.g., to reinforce artificial bone implants, particularly scaffolds for bone tissue engineering made of relatively soft synthetic or natural polymers. In our earlier studies, nanotubes were combined with termoplasts of polytetrafluoroethylene,

polyvinyldifluoride and polypropylene, which significantly enhanced its attractiveness of nanotube-based substrates for colonization with bone-derived cells [23].

Recently, nanotechnology has gained much attention in research to develop new carbon-based materials with unique properties. Nanotechnology can be broadly defined as the creation, processing, characterization and use of materials, devices, and systems with dimensions in the range 0.1–100 nm, exhibiting novel or significantly enhanced physical, chemical, and biological properties, functions, phenomena, and processes due to their nanoscale size [24]. Ultrathin carbon films can be used for analytical applications, e.g. carbon micro-arrays for transmission electron microscopy [25], high resolution microscopy [26], microelectromechanical systems [27] or electrodes for corrosion sensor applications at high temperatures [28]. "Carbon composites" has attracted increasing interest owing to their unique properties and numerous potential applications in the automotive, aerospace, construction and electronic industries [29]. Diamond-like carbon based films on polymer substrates can strongly influence gas barrier performance [30]. Polymer/carbon nanoparticle systems can be used as polar vapour sensors [31]. Thin films on a polymer-fullerene base are used for a hybrid solar cells construction [32]. The intensive investigations of carbon nanolayers and carbon/polymer nanocomposites [33] stimulated remarkably by the discovery of carbon nanotubes [34], fullerenes [35] and graphene layers [36] resulted in the conclusion that the character of the carbon atom connections in the carbon layer has crucial importance for the structure and the properties of carbon nanoparticles and thin layers. Sputtered or evaporated [37] carbon structures can create nanostructures of different electrical or morphological properties. The opportunities for systematic investigation of nanolayers structures [38-42] are very promising for new application both in electronics or nanoengineering and biomedicine.

2. Carbon nanolayers

Thin carbon layers are considered as a prospective material for a wide range of biomedical application [39,43-45], e.g. tissue regeneration [46], controlled drug delivery [47], surface coating for bone-related implants [48], increase of resistance to microbial adherence, blood interfacing implants applications [49] or neuronal growth.

2.1. Carbon layer flash evaporation

Little attention has been devoted to the study of carbon layers prepared by the simplest deposition technique – flash evaporation. By flash evaporation carbon layers of different thickness can be produced for routine SEM and TEM electron microscopy. In general, there is a need for these layers to be fine grain, even coating, with uniform and controllable layer thickness. Flash deposition is distinguished from other techniques (e.g. vacuum evaporation, ion beam) by short deposition time and low total power input. The thickness of flash prepared carbon layer should be controlled, but at present none of the conventional methods in general use allows precise and reproducible deposition and layer thickness

control. Flash deposition can be accomplished either by rapid evaporation of a carbon filament or by pulsed laser vaporization of a carbon target [50]. The former technique is based on rapid evaporation of carbon filament caused by an electric discharge. The majority of the evaporation material is believed to be in the form of molten globules. The carbon layers can be deposited by flash evaporation onto polymer substrates (e.g. PET and PTFE). Their properties are of interest for many potential applications mentioned above and, in our case, for their usage in the study of interaction of living cells with carbonaceous materials and carbon based structures with potential applications in medicine. Physical, chemical and electronic properties of the deposited carbon layer were studied as a function of the distance between the substrate and the carbon source and the layer thickness.

2.1.1. Layer thickness

The dependence of the layer thickness, measured by the scratch technique, on the distance between the substrate and the carbon filaments is shown in Fig. 1 for arrangements with one and two filaments. It is obvious that the layer thickness decreases with deposition distance monotonically, as expected. It should be noted that the deposition process is affected by several phenomena. The filament does not represent a point-like carbon source [51] and during the evaporation process it breaks without fully evaporating along its complete length. The flash evaporation proceeds in rather low vacuum and evaporated carbon particles under a large number of inelastic scattering events with molecules of residual gas on the way from the filament to the substrate, by which their energy is reduced and flight direction is changed randomly.

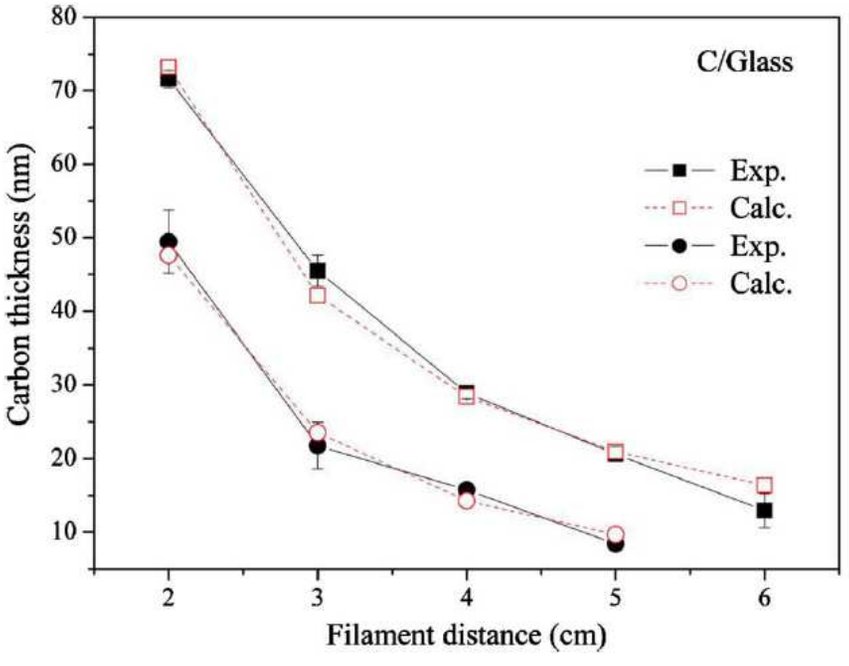

Figure 1. Dependence of the thickness of the flash-evaporated carbon layer on the distance of glass substrate from 1 (circle points) and 2 (square p.) filaments, determined by AFM technique. The values calculated according to formulae presented in [37].

2.1.2. Chemical composition and structure

The typical XPS spectrum of carbon layer deposited onto PTFE is introduced in Fig. 2. One can see that besides of carbon the oxygen is also observed. The presence of oxygen is explained by oxygen absorption from residual atmosphere during deposition process. C1s and O1s peaks correspond to about 94.1 and 5.8 at. % of carbon and oxygen concentration, respectively. The presence of carbonyl, carboxyl and hydroxyl structures in the carbon layer were proved. Hydrogen depth profile was determined by ERDA. It was found that the concentration of carbon and hydrogen decreases with increasing depth while the concentration of fluorine increases. No hydrogen is detected beyond 75 nm. This observation may indicate that the thickness of deposited carbon layer is about 75 nm (in accordance with measurements performed on glass samples) and at larger depths the composition approaches pristine PTFE [37].

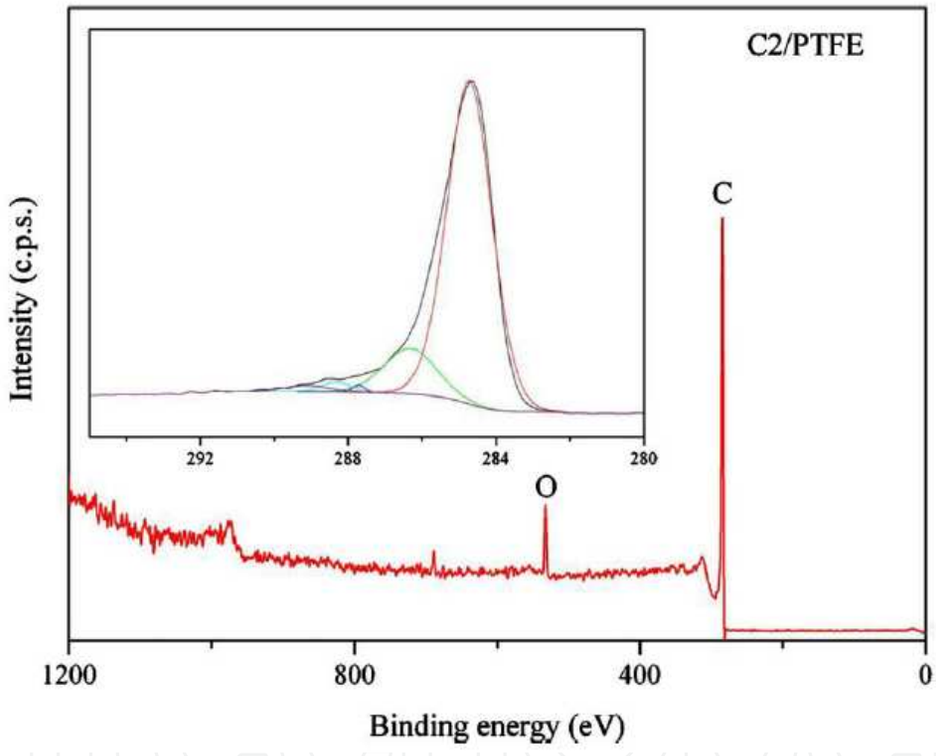

Figure 2. XPS spectrum of the carbon layer deposited from 2 cm distance on PTFE; decomposition of the O1s band is shown too [37].

2.1.3. Surface properties

Surface wettability depends on surface chemical structure [52] and is commonly characterized by contact angle. Contact angle on polymers was studied as a function of the distance of PET and PTFE substrates from the filament. It was observed on PTFE substrate that the contact angle increases with an increasing deposition distance (thinner layer thickness), while on PET the contact angle does not change within experimental errors for deposition distances from 2 to 7 cm. According to XPS analyses chemical composition of the deposited carbon layer is the

same for both polymers with low concentration of oxidized, polar structures. It is supposed that the wettability might also be affected by surface morphology and roughness of both polymers. While the roughness of PET after carbon coating remains unchanged within experimental error, a dramatic change of the roughness is observed on PTFE. With increasing thickness of the carbon layer the PTFE roughness decreases from 13.3 nm for pristine PTFE to 2.9 nm for thickest layer (deposition from 2 cm). Significant differences in the surface morphology are found between both polymers before and after carbon deposition (see Fig. 3). For pristine PET the surface is composed of tiny, rounded formations, homogenously distributed over the sample surface. Carbon deposition does not result in any significant change in the surface morphology and roughness. Surface of the pristine PTFE is markedly wrinkled and its roughness is higher comparing to PET. Carbon deposition results in a dramatic morphology change and roughness declines indicating a preferential carbon accumulation into holes.

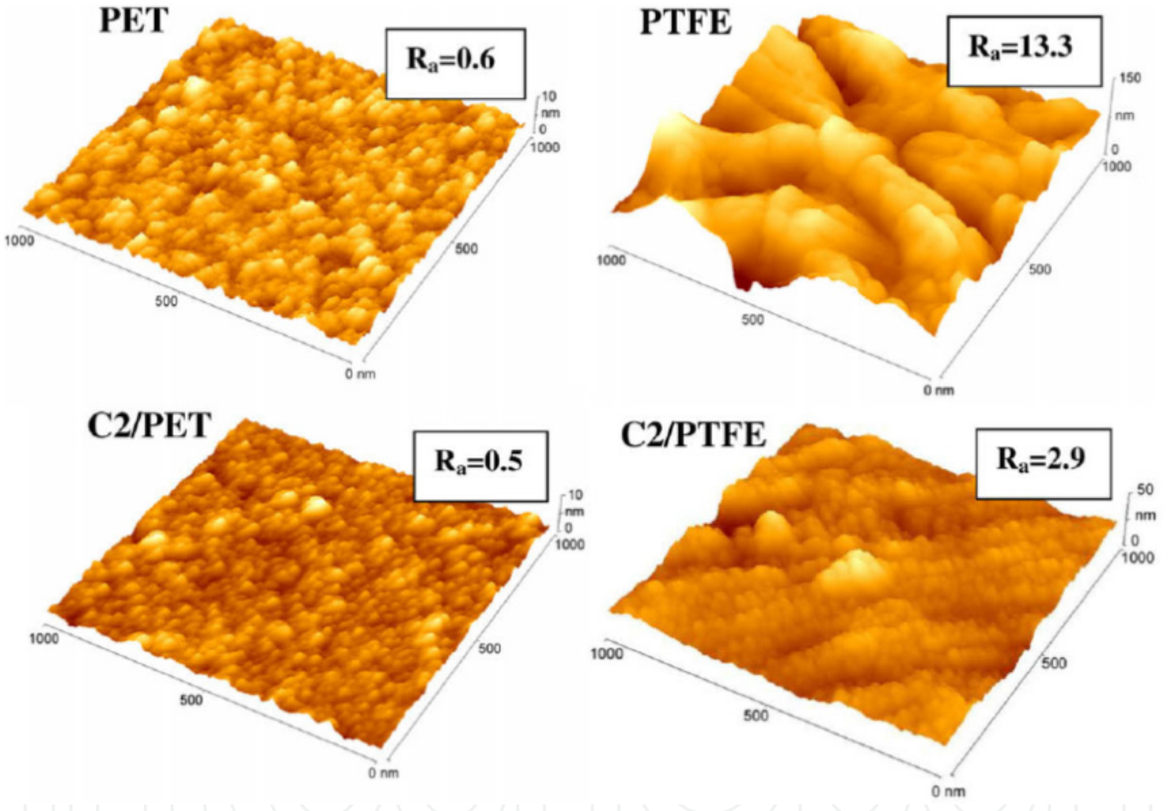

Figure 3. AFM images of pristine PET and PTFE and those coated with carbon from the deposition distance of 2 cm (C2/polymer). R_a is surface roughness in nm [37].

2.1.4. Electrical properties

Carbon deposition results in a rapid resistance decrease (comparing to pristine polymers) indicating formation of continuous carbon layer on the polymer. The decrease of electrical sheet resistance (R_s) is more pronounced on PET, probably due to lower surface roughness. According to our previous results [37] the conditions of the layer deposition were chosen to obtain about 70 nm thick carbon layers. For the measurement of the sheet resistance R_s as a function of the temperature, the C/PTFE samples were placed in the cryostat cooled by LN_2.

Temperature dependence of the sheet resistance, measured in the temperature range from 80 to 350 K, is shown in Fig. 4a. One can see that over a broad temperature range the sheet resistance decreases rapidly with increasing temperature. The decrease is typical for semiconductors; "semiconductance" of amorphous carbon (a-C) was reported earlier, e.g. in [53]. It is believed that the mechanism of the charge transport in carbon layers proceeds according to variable range hopping (VRH) mechanism, suggested by Mott [54], which depends on the density of the states present near the Fermi level. The same dependence as in Fig. 4a is shown in Fig. 4b in ln $R_s(T)$ vs. $T^{-1/4}$ representation. One can see that the VRH model describes well the charge transport in the temperature range from 80 to 350 K. It is supposed that the electron states are localised on carbon clusters sp^2, dispersed randomly within the carbon layer. After application of an external electrical field electron hopping between the clusters takes place. The electron movement proceeds via phonon-assisted tunneling and with decreasing temperature the electrons tend to hop to larger distances on sites which are energetically closer than the nearest neighbour.

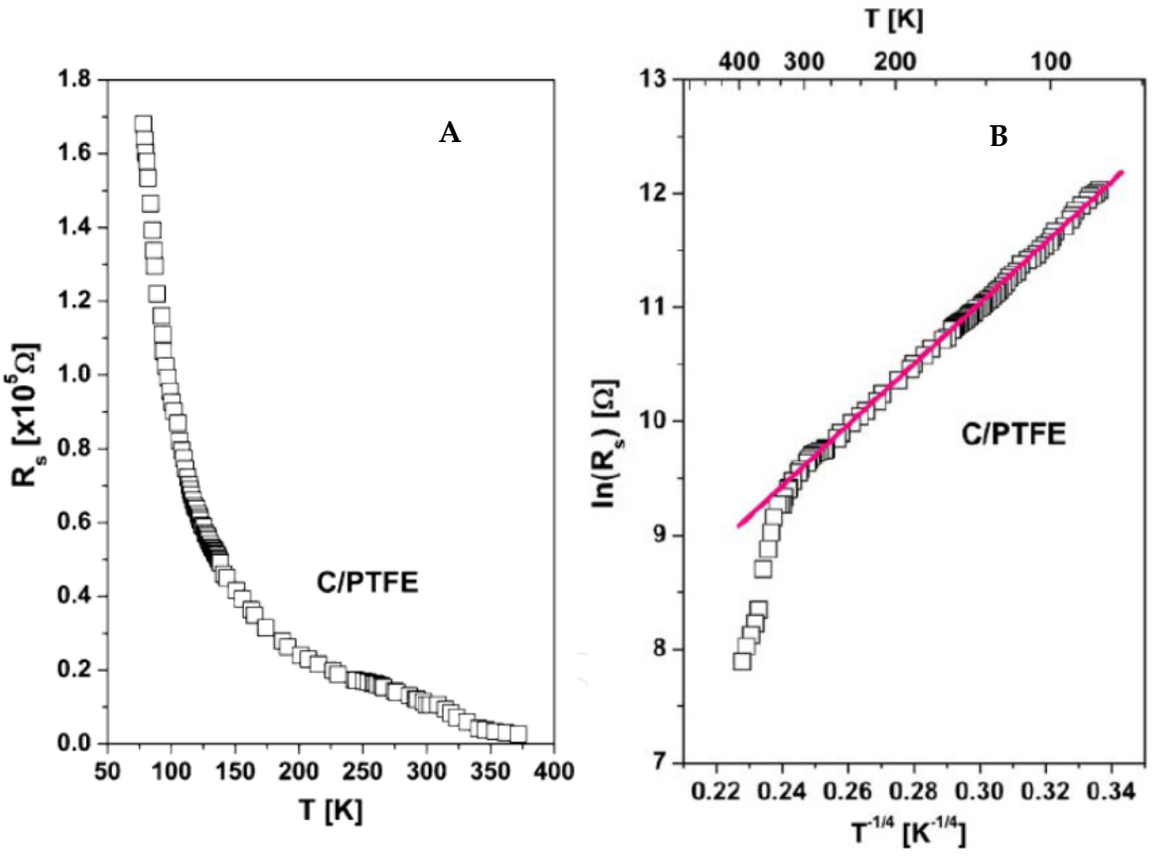

Figure 4. Temperature dependence of the sheet resistance (R_s) for carbon layer, 70 nm thick, flash evaporated onto PTFE (a) and temperature dependence of the sheet resistance R_s in form ln R_s vs. $T^{-1/4}$ (b) for the same sample [41].

2.1.5. Zeta potential

Electrokinetic analysis results of flash deposited carbon layers on PTFE are presented in Fig. 5 [41]. It is clear, that after carbon deposition decreases zeta potential obtained by

Helmholtz-Smoluchowski equation due to creation of carbon layer. Carbon layers embody the similar behavior as gold layer [55]. The thicker carbon layer the lower zeta potential value. Results for sample distance of 4 and 7 cm are the same due to similar value of surface roughness [41]. After deposition from distance 2 cm zeta potential dramatically decreases due to significant decrease of thickness of carbon layer, surface roughness and sheet resistance. Difference between zeta potential obtained by both of used methods and equations (streaming current, Helmholtz-Smoluchowski eq. and streaming potential, Fairbrother-Mastins eq. [41]) is significant for pristine PTFE due to great surface roughness. For other samples this difference increases with decreasing distance of filaments. It can be explained by increasing surface conductivity, which plays an important role in zeta potential calculation and comparison. Zeta potential obtained by Fairbrother-Mastins equation increases due to increasing polarity of surface, which is explained by creation of polar groups on surface. It can be concluded from Fig. 5 that carbon layer deposited from distance 2 cm is the most conductive.

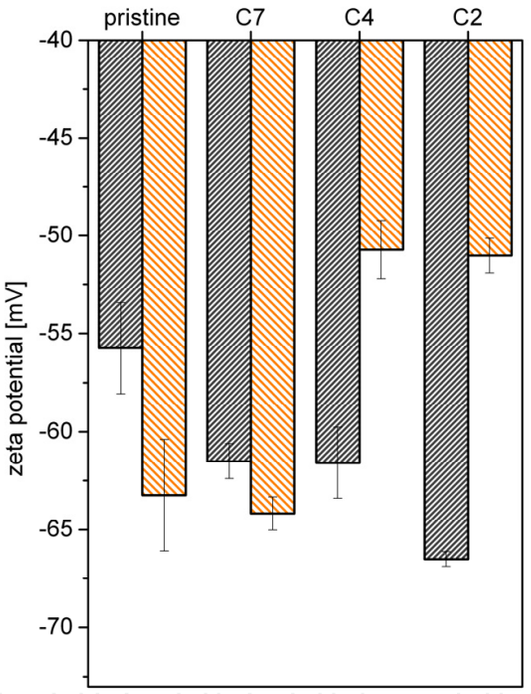

Figure 5. Zeta potential of pristine PTFE (pristine) and PTFE with carbon flash evaporated layer from distances 2, 4 and 7 cm (C2, C4 and C7). Black columns represent data obtained by streaming current method (Helmholtz-Smoluchowski equation), the orange ones by streaming potential (Fairbrother-Mastins equation) [41].

2.1.6. Cell adhesion and proliferation

Cytocompatibility of samples was determined from *in vitro* experiments on adhesion and proliferation of LEP cells (human diploid fibroblastoids) performed on pristine and carbon coated PTFE. For comparison the same experiments were performed on „tissue polystyrene“ (PS) too. The results are presented in Fig. 6. It is seen that the carbon coating increases adhesion and proliferation (Fig. 6) of LEP cells significantly in comparison with pristine PTFE [41].

Cell proliferation 3 days after the seeding is comparable with tissue PS. For both cell adhesion and proliferation maximum positive effect is seen on the samples carbon coated from the distance 4 cm. In this case the carbon layer is about 32 nm thick and it exhibits the higher roughness, good electrical conductivity and contact angle of about 80°. Low surface roughness and wettability seem to have negative effect on the cell adhesion and proliferation [41].

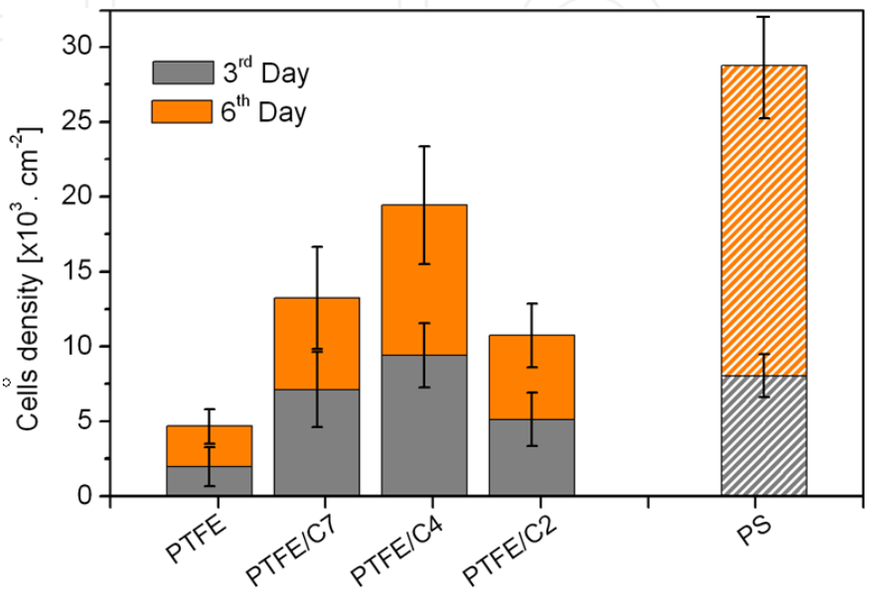

Figure 6. The proliferation of LEP cells proliferation (3rd and 6th day) on pristine PTFE, PTFE with carbon layers prepared by carbon flash evaporation from the distances 2, 4 and 7 cm (C2, C4 and C7) and on the „tissue" polystyrene PS [41].

2.2. Carbon layer sputtering

Different types of carbon layers can be preferentially prepared by various types of carbon deposition. DLC films can be deposited using DC plasma chemical vapor deposition, radio frequency magnetron sputtering or ion beam-based methods. DLC (polycrystalline diamond) needs high temperatures to be deposited [56]. Amorphous carbon can be prepared at low temperatures by different techniques, but its physical, chemical and mechanical properties depend on the deposition conditions, mainly on the temperature and hydrogen content [57]. Hydrogenated amorphous carbon (a-C:H) is usually prepared by plasma-assisted CVD of hydrocarbons (i.e. methane or ethylene). Amorphous carbon (a-C) is prepared by PVD techniques such as sputtering, arc discharge or pulsed laser deposition. Amorphous hydrogenated carbon is unstable under thermal treatment since it tends to eliminate hydrogen and transform in to a more stable graphitic structure. As an alternative method for thin layer preparation the sputtering method was chosen. Carbon layers on polyethyleneterephtalate (PET) backing were prepared by sputtering from graphite target. The deposited layers were characterized by different techniques (UV-VIS, Raman spectroscopy, RBS, AFM) and the biocompatibility of the layers was studied by cultivation of 3T3 mouse fibroblasts.

2.2.1. Structure of sputtered carbon layers

UV-VIS spectrometry is used frequently to follow the changes in chemical structure of polymers. Absorbance increase indicates an increase of the concentration of structures with certain length (number) of conjugated double bonds. Longer structures absorb on longer wave lengths [58]. It was determined that the amount of π bonds (sp^2 hybridization) and the length of conjugated double bonds are increasing functions of the sputtering time. The thickness of the deposited carbon layer increases with increasing sputtering time as could be expected. The structure of the carbon layers can be characterized by Raman spectroscopy [59]. Raman peak at 1360 cm^{-1} is attributed to disordered mode of graphite and that at 1500–1550 cm^{-1} corresponds to an amorphous-like structure with sp^3 + sp^2 bonding [59]. Fig. 7 shows the Raman spectra from pristine PET and PET with carbon layer deposited for 30–90 min. The carbon deposition for the times up to 30 min does not result in any observable changes in the spectra. The deposition for longer times leads to appearance of a signal in 1100–1700 cm^{-1} region, the intensity of the signal being an increasing function of the deposition time. All spectra exhibit a broad peak at 1530 cm^{-1} indicating that the deposited layers are composed mostly of amorphous carbon with sp^3 and sp^2 bonds. Small peak at 1360 cm^{-1}, which is also present in all spectra, is due to the presence of disordered graphite. The results of Raman and UV-VIS spectroscopy show that the thickness of the deposited layers increases with increasing sputtering time.

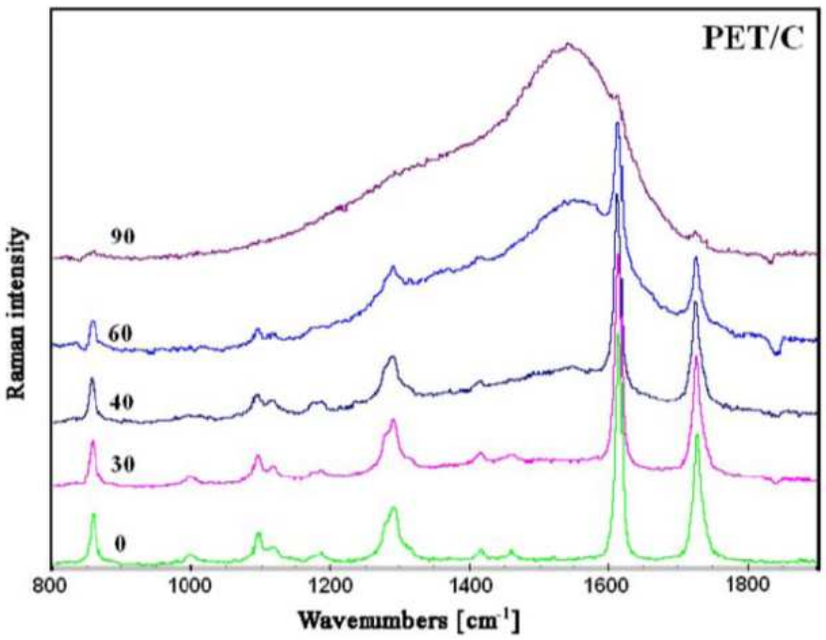

Figure 7. Raman spectra from pristine PET and PET samples with carbon layers deposited for different sputtering times (min) as indicated in the figure [45].

ERDA (Elastic Recoil Detection Analysis) revealed information on hydrogen concentration and its depth profile in the deposited layers. RBS spectra provided information on carbon and oxygen concentration and on the layer total thickness. It was observed that for the sputtering times above 45 min the composition of the deposited layers does not depend,

within RBS and ERDA experimental errors, on the deposition time. The measured concentrations varied from 7 to 9 at. % for oxygen and from 16 to 26 at. % for hydrogen. These concentrations were significantly lower than those in pristine PET. The layer thickness increased roughly linearly with increasing deposition time.

The layer morphology changes as a function of the sputtering time and the layer thickness. It was found that after 15 s of deposition carbon creates rounded, regular grains the size of which is larger compared to those observed for longer sputtering times [45]. For the sputtering times above 30 s the carbon grains become smaller but some irregularities arise. The surface roughness is an increasing function of the deposition time.

2.2.2. Cell growth

The carbon layers-PET structures were used as a substrates for cultivation of 3T3 mouse fibroblasts (Fig. 8) [38]. The number of adhering cells increases with increasing deposition time for deposition times up to 30 min (Fig. 9). For longer deposition times on the contrary the cell number decreases with increasing deposition time (Fig. 9). Possible explanation of the decline may be found in unfavourable surface morphology and roughness of the layers deposited for longer times. Possibly the adhering cells prefer smooth surface without sharp irregularities. An effect of the layer continuity or discontinuity can not be excluded, too. It should also be noted that in the present case a non-polar material (carbon) is deposited onto polar substrate. The surface modification of PET by carbon has the positive influence on cells adhesion and sample sputtered 30 min has the greatest amount of adhered cells.

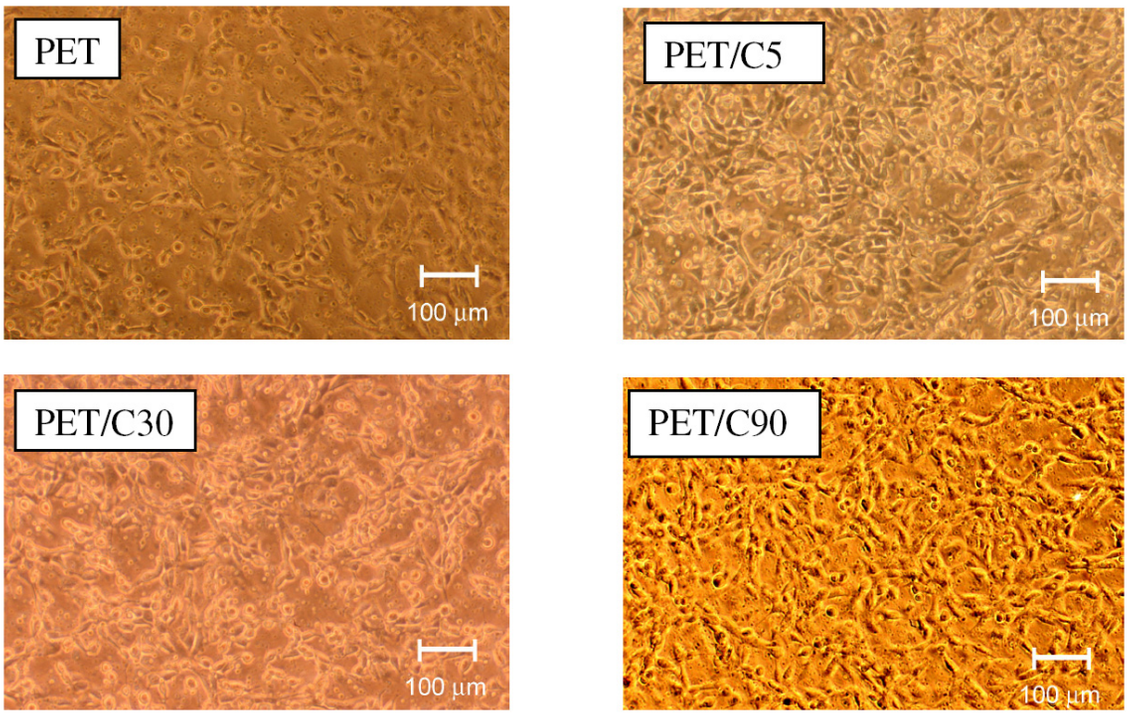

Figure 8. Cells distribution on PET with different time of carbon deposition. The equable distribution of the 3T3 fibroblasts on the PET after carbon deposition is shown [38].

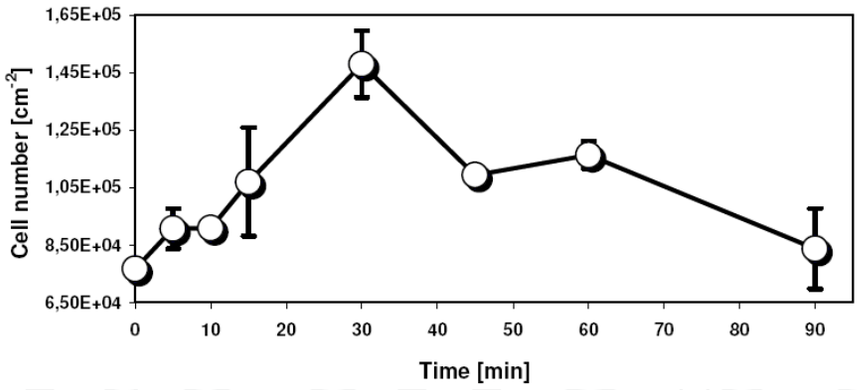

Figure 9. Dependence of number of cells on the time of carbon deposition by magnetron sputtering on the PET [38].

2.3. Fullerenes

Above other interesting properties, fullerenes emit photoluminescence which could be utilized in advanced imaging technologies [60]. In their pristine unmodified state, fullerenes are highly hydrophobic and water-insoluble. On the other hand, they are relatively highly reactive, which enables them to be structurally modified. Fullerenes can form complexes with other atoms and molecules, e.g. metals, nucleic acids, proteins, synthetic polymers as well as other carbon nanoparticles, e.g. nanotubes. In addition, fullerenes can be functionalized with various chemical groups, e.g. hydroxyl, aldehydic, carbonyl, carboxyl, ester or amine group, as well as amino acids and peptides. This usually renders them soluble in water and intensifies their interaction with biological systems [61]. Despite all these exciting findings, relatively little is still known about the influence of fullerenes, particularly when arranged into layers and used for biomaterial coating, on cell-substrate adhesion, subsequent growth, differentiation and viability of cells, especially bone-forming cells.

2.3.1. Physical and chemical properties of fullerene C_{60} layers

Fullerenes C_{60} were deposited onto microscopic glass coverslips by evaporation of C_{60} in the Univex-300 vacuum system (Leybold, Germany). The thickness of the layers increased proportionally to the temperature in the Knudsen cell and the time of deposition. Four types of layers of different thickness and morphology were prepared: thin continuous, thick continuous, thin micropatterned and thick micropatterned. The micropatterned layers were created by deposition of fullerenes through a metallic mask with rectangular holes [62].

Raman analysis was performed on micropatterned samples immediately after deposition and then after sterilization with ethanol. Immediately after deposition, the Raman spectra showed that the fullerene films were prepared with high quality [62]. After sterilization with ethanol, the thin micropatterned fullerene layers were almost intact, and a considerable amount of fullerenes was found not only on sites underlying the openings of the grid, but also below its metallic part. However, in thick micropatterned layers, an analysis of the vibration mode showed that the C_{60} molecules reacted with oxygen or polymerized [62].

The proportion of C_{60} molecules involved in these chemical changes and reached about 50%. Moreover, the amount of fullerenes below the metallic bars of the grid was very low, though still detectable. The color intensity increased with layer thickness, while the transparency of the layers in a conventional light microscope decreased [62]. Despite of this, the cells on both continuous layers were well observable, even those native and non-stained (Fig. 9A–D). On thick micropatterned layers, the bulge-like prominences were relatively dark, and the contrast between the bulges and grooves was relatively high (Fig. 9E). In addition, it was not possible to focus the cells on bulges and in grooves simultaneously, whereas the fluorescence signal from both groups of cells was observable. Thus, the presence and morphology of cells on bulges and in grooves was evaluated using fluorescence microscopy (Fig. 9F).

Reflection goniometry showed that all fullerene C_{60} layers were relatively highly hydrophobic. The continuous and micropatterned layers had similar water drop contact angles ranging from 95.3 ± 3.1° to 100.6 ± 6.8°.

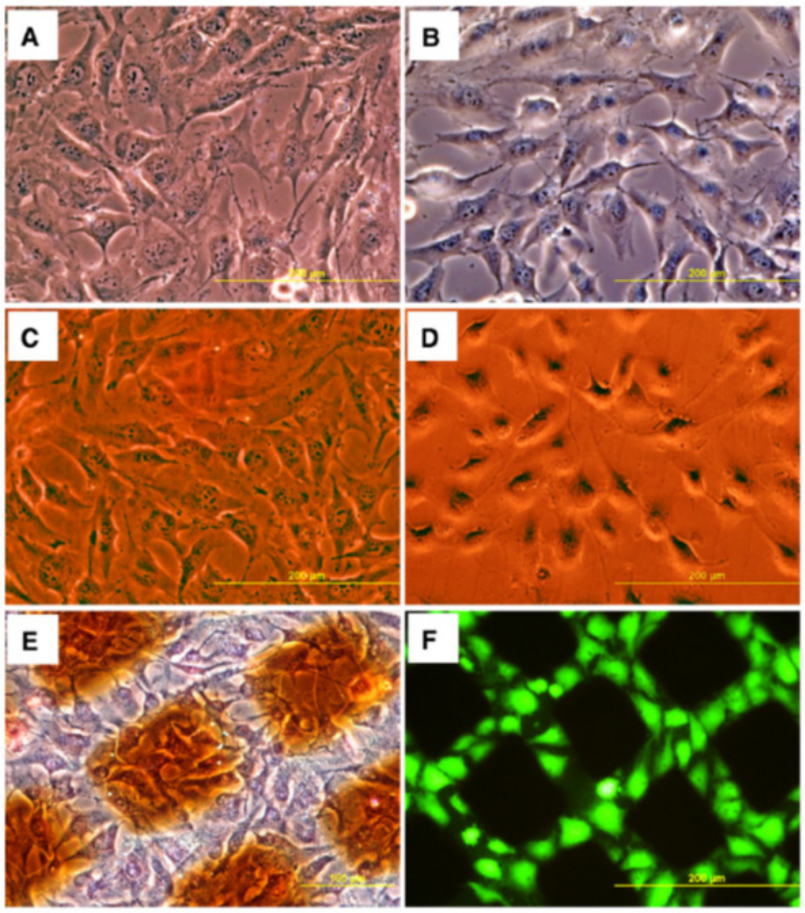

Figure 10. Morphology of human osteoblast-like MG 63 cells in cultures on a polystyrene dish (A) a microscopic glass coverslip (B), thin continuous (C), thick continuous (D), thin micropatterned (E) and thick micropatterned (F) fullerene C60 layers. A–D: native cultures; E: a culture stained with hematoxylin and eosin; F: a culture stained with LIVE/DEAD viability/cytotoxicity kit (Invitrogen). A–D: day 5 after seeding, E–F: day 7 after seeding. Olympus IX 50 microscope, DP 70 digital camera, obj. 20x, bar=200 μm except E, where bar=100 μm [62].

2.3.2. Adhesion and proliferation of cells

On day 1 after seeding, the cells on both continuous thin and thick fullerene layers adhered at similar numbers (3420±420 cells cm^{-2} and 2880±440 cells cm^{-2}, respectively), which was comparable to the values found on standard cell culture substrates, represented by the tissue culture polystyrene dish (3080±290 cells cm^{-2}) and the microscopic glass coverslip (2560±310 cells cm^{-2}) [62]. On both micropatterned thin and especially thick fullerene layers, the average cell population densities tended to be lower (by 11 to 43 %) than both polystyrene and glass, but these differences were not statistically significant. The cells colonized practically exclusively the grooves (Fig. 9F), thus they used less space for their proliferation. Although the grooves occupied only 41±1 % of the material surface, they contained from 80±4 % to 98±1 % of the total cells on the material surface [62]. The cell population density in the grooves was about 5 to 57 times higher than on the bulges, and these differences increased with time of cultivation. On the other hand, on the thin micropatterned films, the cells colonized homogeneously the entire surface of the sample (Fig. 9E) and the percentage as well as the population density of cells in the grooves and on the bulges were similar.

2.3.3. Presence and spatial arrangement of β1-integrins, talin, β-actin and osteopontin

As revealed by immunofluorescence, MG 63 cells on both continuous and micropatterned fullerene layers were intensively stained for β1 integrins and talin, i.e. molecules participating in cell-substrate adhesion, β-actin, an important component of the cytoplasmic cytoskeleton, as well as osteopontin, a marker of osteogenic cell differentiation. This staining intensity was similar as in cells on the control polystyrene culture dish and microscopic glass coverslips (Fig. 10). All these molecules (particularly extracellular matrix protein osteopontin) were found in fine granular distribution throughout the cells, often preferentially located in the perinuclear region [62]. In addition, both β1 integrins and talin also formed dot- or streak-like focal adhesion plaques, visible mainly on the cell periphery.

Beta-1 integrin-containing focal adhesion plaques were particularly well developed and were often located on fine long protrusions formed by cells, which was accompanied by the formation of a fine mesh-like β-actin cytoskeleton. No apparent differences in the staining intensity and distribution of all molecules mentioned here were found between cells growing on thin and thick micropatterned fullerene layers or in cells in grooves and on bulges [62].

2.4. Carbon nanoparticles

Carbon nanoparticles, nanotubes and nanodiamonds, are considered as promising building blocks for the construction of novel nanomaterials [63,64] for emerging industrial technologies, such as molecular electronics, advanced optics or storage of hydrogen as a potential source of energy. In addition, they are considered as promising materials for biomedical applications, such as photodynamic therapy against tumors and infectious agents, quenching oxygen radicals, biosensor technology, simulation of cellular components, such as membrane pores or ion channels, as well as controlled drug or gene delivery,

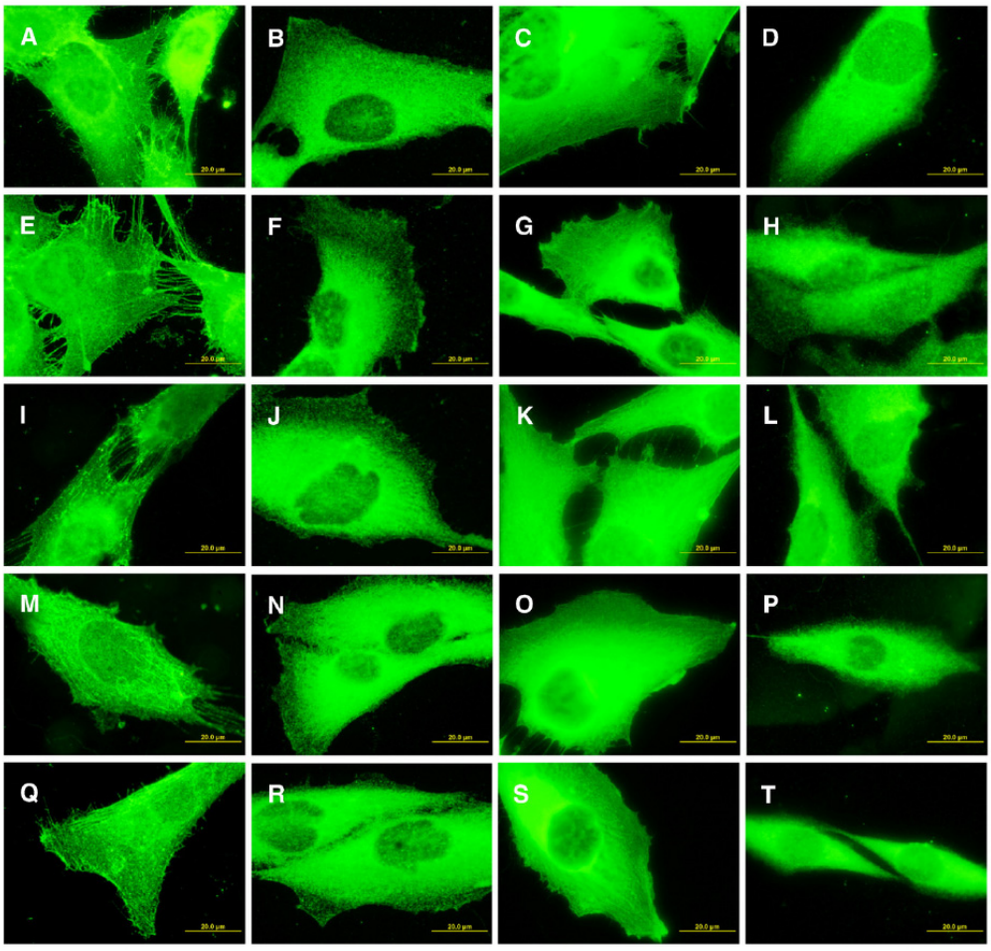

Figure 11. Immunofluorescence staining of β1 integrins (A, E, I, M, Q), talin (B, F, J, N, R), β-actin (C, G, K, O, S) and osteopontin (D, H, L, P, T) in human osteoblast-like MG 63 cells on day3 after seeding on microscopic glass coverslips (A–D), thin continuous (E–H), thick continuous (I–L) thin micropatterned (M–P) and thick micropatterned (Q–T) fullerene C60 layer. Olympus epifluorescence microscope IX 51, digital camera DP 70, obj. 100×, bar=20 μm [62].

particularly targeting the mineralized bone tissue [65]. Despite these exciting perspectives, relatively little is known about the influence of carbon nanoparticles present on the biomaterial surface on the adhesion and growth of cells.

Therefore the three types of materials modified with carbon particles were prepared: (i) carbon fibre-reinforced carbon composites (CFRC), materials promising for hard tissue surgery, coated with a fullerene C_{60} layer, (ii) terpolymer of polytetrafluoroethylene, polyvinyldifluoride and polypropylene mixed with 4 wt. % of single or multi-walled carbon nanotubes and (iii) nanostructured or hierarchically micro- and nanostructured diamond layers deposited on silicon substrates [23].

The materials were seeded with human osteoblast-like MG 63 cells (density from 8500 cells cm^{-2} to 25 000 cells cm^{-2}) [23]. On the fullerene layers, the cells (day 2 after seeding) adhered in number from 2.3 to 3.5 times lower than those on control non-coated CFRC or polystyrene dishes. However, their spreading area was larger by 68 % to 145 % than that on

the control surfaces. On diamond layers, the number of initially adhered cells was higher on the nanostructured layers, whereas the subsequent proliferation was accelerated on the layers with a hierarchical micro-and nanostructure [23].

2.4.1. Carbon fibre-reinforced carbon composite (CFRC)

Carbon fibre-reinforced carbon composite (CFRC) was coated with fullerene layer. The fullerene coating did not significantly change this surface microroughness but created a nanostructured pattern on the pre-existing microarchitecture of the CFRC surfaces. The contact angle was unmeasurable due to a complete absorption of the water drop into the fullerene layer, which suggested a certain non-compactness or porosity of this layer. The contact angle of the non-coated CFRC was 99.5±1.0°. The release of fullerenes into the culture media and their cytotoxic action seemed to be less probable in our experiments. The cell attachment and spreading on the uncoated regions of them fullerene-modified CFRC, and also on the bottom of the polystyrene dishes containing fullerene-coated samples, were similar as in the control polystyrene dishes without fullerene samples. At the same time, the fullerene layer was resistant to mild wear, represented by swabbing with cotton, rinsing with liquids (water, phosphate-buffered saline, culture media) and exposure to cells and proteolytic enzymes used for cell harvesting. After these procedures and/or one-year-storage at room temperature in dark place, the Raman spectra did not change significantly [23]. On day 2 after seeding, the cell population density (Fig. 11A) on the CRFC surfaces was lower than that on the control uncoated material and TCPS, which could be due to the relatively high hydrophobicity of the non-functionalized fullerenes. In addition, the fullerene-coated CFRC surfaces were stronger and less prone to release carbon particles, which is an important limitation of the potential biomedical use of CFRC [66]. Moreover, the spreading area of cells on the fullerene-coated samples amounted to 3,182 ± 670 mm^2, while on both control surfaces it was only 1888 ± 400 and 1300 ± 102 mm^2 (Fig. 11B). This could be explained by the low cell population density on the fullerene layer, which provided the cells with more space for them to spread [23].

2.4.2. Carbon nanotube–polymer composites

Similarly as on the fullerene layer, the cells on PTFE/PVDF/PP mixed with single-wall carbon nanohorns (SWNH) or multiwall nanotubes (MWNT-A) were well spread, polygonal, and contained distinct beta-actin filament bundles, whereas most cells on the pure terpolymer were less spread or even round and clustered into aggregates [23]. The enzyme-linked immunosorbent assay (ELISA) revealed that the cells on the material with SWNH contained a higher concentration of vinculin and talin, i.e. components of focal adhesion plaques. While on day 1 after seeding the initial cell population density was similar on the terpolymers with or without MWNT-A, on day 7, the cells on the MWNT-A-modified terpolymer reached a density 4.5 times higher than the density on the unmodified samples (Fig. 11C). The improved adhesion and growth of MG 63 cells on the nanotube-modified terpolymer could be attributed to changes in its surface roughness rather than to its surface wettability, which remained unchanged and relatively low [23].

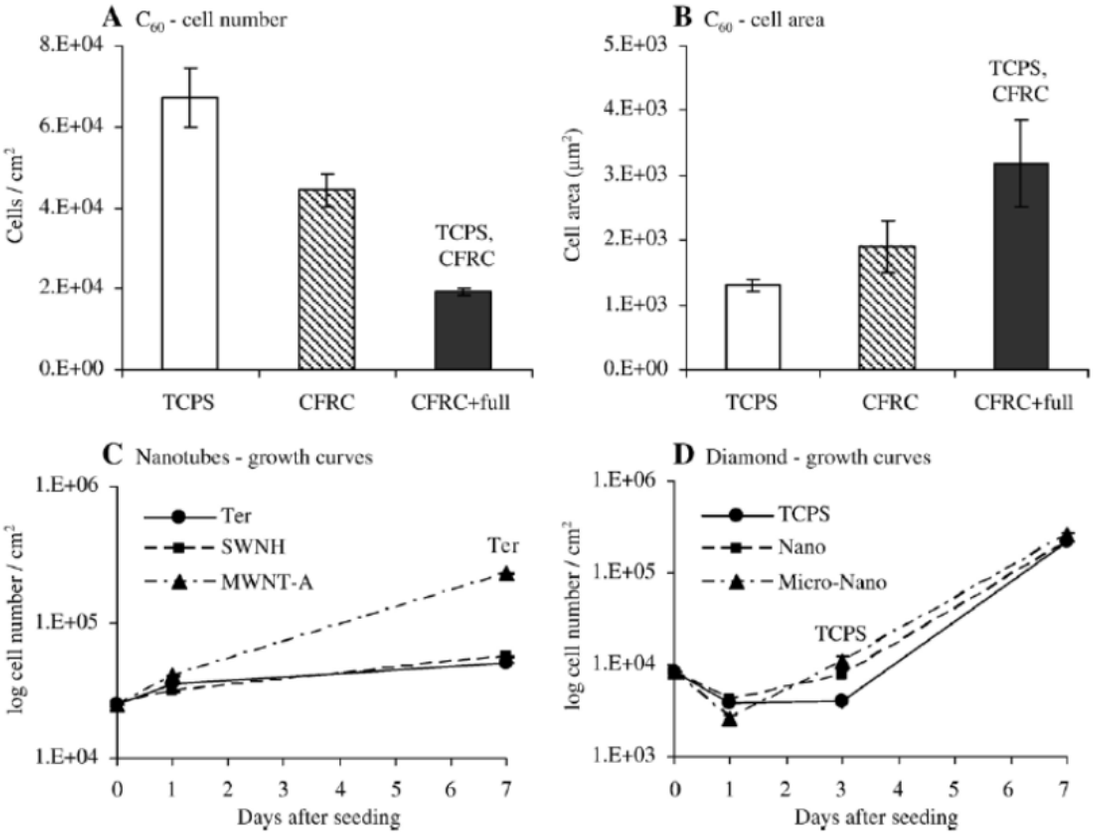

Figure 12. Population density (A) and adhesion area (B) of osteoblast-like MG 63 cells on day 2 after seeding on tissue culture polystyrene dish (TCPS), carbon fibrereinforced carbon composites (CFRC) and CFRC coated with a fullerene layer (CFRC+full). C: Growth curves of MG 63 cells on a terpolymer of polytetrafluoroethylene, polyvinyldifluoride and polypropylene (Ter), terpolymer mixed with 4 wt. % of single-wall carbon nanohorns (SWNH) or 4 wt.% of high crystalline electric arc multi-wall nanotubes (MWNT-A). D: Growth curves of MG 63 cells on TCPS, a nanostructured diamond layer (Nano) and a layer with hierarchically organized micro-and nanostructure (Micro-Nano). Mean±S.E.M. from 4–12 measurements, ANOVA, Student–Newman–Keuls method. Statistical significance: TCPS, CFRC, Ter: $p \leq 0.05$ compared to the values on tissue culture polystyrene, pure CFRC and pure terpolymer [23].

2.4.3. Diamond layers

On nanostructured diamond layers, the number of initially adhered cells on day 1 after seeding was similar to that found on the control TCPS (Fig. 11D), whereas on the layers with a combined micro and nanoarchitecture, this number was significantly lower. In addition, the cells on the latter samples were distributed non-homogeneously [23]. However, from day 1 to 3 after seeding, the cells on the hierarchically micro- and nanostructured layers, which are considered to resemble the architecture of natural tissues, showed the quickest proliferation. Their doubling time was 23.4 h, whereas on the nanostructured layers, it was 56.7 h, and on TCPS, the cells still remained in the lag phase and have not yet started their proliferation [23]. As a result, on day 3 after seeding, the cells on the diamond layers with a combined micro-and nanostructure reached the highest cell population density compared to nanostructured diamond and TCPS, respectively [23].

2.5. Chemical vapour deposition

Another type of carbon layer useful for the preparation of biocompatible surfaces includes chemical and physical vapor deposition. The preparation of the carbon layers on polytetrafluoroethylene (PTFE) by photoinduced CVD from acetylene and their physical properties and chemical structure have been studied. These properties related to the adhesion and proliferation of human umbilical endothelial cells (HUVEC) seeded thereon were characterized [39].

2.5.1. Surface morphology and layer thickness

The surface morphology was changed during the photo-deposition by carbon. The images suggest that in a first step the surface is covered by carbon and then the holes present in the material are filled. However, one should keep in mind that due to the production process the surface of pristine PTFE foils are typically not very homogeneous regarding surface roughness. The main difference is between the pristine PTFE and PTFE/C. The surface roughness is decreasing after more than 20 min deposition [39].

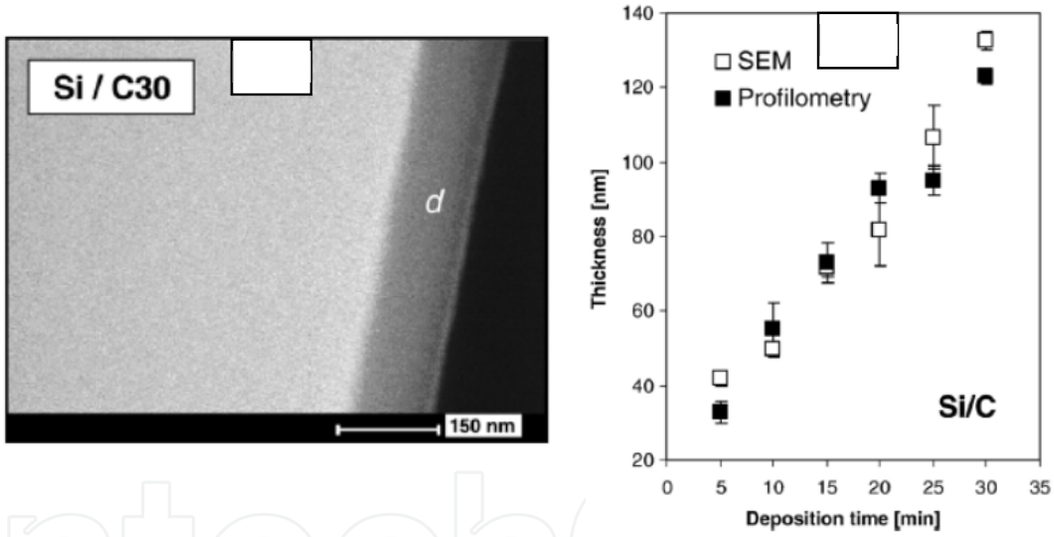

Figure 13. SEM scan of the carbon layer (d=thickness, gray shadow part) deposited 30 min on a silicon substrate (bright white part, left) (A) and the thickness dependence of the carbon layers on the deposition time. (B) The thickness was measured on Si substrate by SEM and profilometry [39].

The thickness of the deposited layers was measured by SEM microscopy and profilometry [39]. For both methods silicon platelets were used as substrates. For SEM microscopy, the coated Si platelets were broken and such a cross-section can be obtained. Fig. 14A shows the SEM cross-section of a broken Si sample coated with carbon for 30 min. The silicon substrate is represented by the bright white part on the left of the image, while the gray shadow part represents photo-deposited carbon layer. The dependence of the carbon layer thickness on deposition time measured by SEM and by profilometry is presented in Fig. 14B. Data of both methods show a nearly linear increase of the thickness with the deposition time.

2.5.2. Surface wettability and chemical stability

Surface wettability can be characterized by water contact angle, mainly influencing adhesion of cells on the modified polymer [45]. Pristine PTFE is a strongly hydrophobic material with a very high contact angle. With increasing carbon deposition time, the water contact angle strongly decreases to values considerable below 90°, which is a typical value for hydrocarbons. As discussed later, we attribute this decrease of the contact angle below 90° to polar groups in the carbon layers. There may be also effects of the surface roughness.

2.5.3. Surface chemistry

The results from Raman spectroscopy (whole layer thickness) and XPS (only surface layer) indicated, that the photoinduced deposition from acetylene results in layers consisting of C-H, C-C, C=C, C=O and O-H it means also C-O-H) bonds. The oxygen containing groups are probably either formed due to reactions layer with residual gases in reaction chamber or due to oxidation of unsaturated radicals by the exposure of samples to air after the deposition. The occurrence of polar oxygen containing groups and remaining radicals are suggested to be the main reason for the low water contact angle [45].

2.5.4. Cell-surface interaction

HUVEC were seeded on the pristine PTFE and PTFE coated with different carbon layers [45]. The adhesion was studied after 1 day, the proliferation after 3 and 7 days. The amount of cells was determined by counting from images and MTS test [39]. The positive influence of the photo-deposited carbon layer for cytocompatibility is more significant after 3 and even more after 7 days of proliferation. The highest cell densities were detected after 7 days on the sample with a deposition time of 20 min. The phase-contrast micrographs of HUVEC on various samples 7 days after seeding revealed only a relative small number of cells adhered pristine PTFE. The cells have a small diameter and a round shape and seem to try to avoid the contact with the surface. On the other hand on carbon coated PTFE, the number of cells was much higher. The highest amount of cells is significant on the sample coated for 20 min by carbon. Here the cells were spreaded onto surface and had a polygonal shape. The large difference in cell adhesion and proliferation between pristine PTFE and carbon coated PTFE allows to confine the cells to certain areas at the surface. This is demonstrated in Fig. 15, where the sample was covered during carbon deposition by a contact mask with 1.5 mm diameter holes. The cells practically only adhere and proliferate at the carbon coated spot.

2.6. One substrate, three deposition methods

2.6.1. Thickness, contact angle and resistance of deposited C-layers

For the comparison of deposition methods the samples with approximately the “same” thickness (interval 73-85 nm) were chosen. From the values of contact angle measured with water drop presented we can resume that the most hydrophobic is pristine PET. Due to coverage of the substrate by the carbon layers we observed lower values of contact angle. This

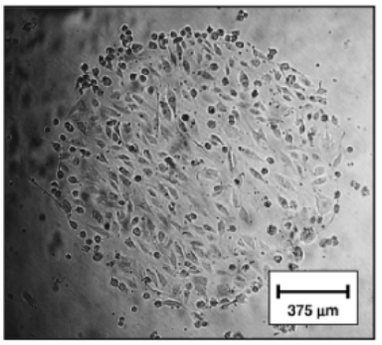

Figure 14. Phase-contrast micrographs of HUVEC (7 days after cell seeding) on a sample coated selectively with carbon for 20 min by photo-induced CVD through a contact mask (spot diameter 1.5 mm) [39].

fact shows an increase of hydrophilic character of the carbon layers. The concentration of carbon, oxygen and nitrogen in PET and carbon layer deposited by evaporation, sputtering and CVD deposition was determined. The samples prepared by sputtering contained the most amount of oxygen in comparison with others deposited carbon samples. This means that sputtered layer is containing more polar oxygen groups, but still it is showing higher contact angle. It is known that polarity or wettability of the surface [67] is determined also by other parameters for example surface roughness and morphology which will be discussed later.

2.6.2. Surface morphology of deposited C-layers

It was observed that carbon layer evaporation did not cause significant change of the surface morphology of pristine PET. The values of roughness R_a were comparable for the pristine PET and evaporated PET. The higher values of R_a were typical for the samples prepared by sputtering and CVD method. The surface morphology was changed dramatically during the photo-deposition by carbon. It is seen that the morphology of the evaporated and sputtered layers are similar instead of layer after CVD from acetylene. The sharp areas on the sample prepared by CVD method were not found on the others.

2.6.3. Chemical structure of deposited carbon layers

The Raman spectra of pristine PET and carbon layers on PET prepared by evaporation, sputtering and CVD methods are shown in Fig. 16. The spectra have differences especially between 3000-2750 cm^{-1} where some characteristic peaks are present in the spectrum of CVD: 2931 cm^{-1} is typical for C-H vibration from -CH_2- groups, a weak band at ca. 3040 cm^{-1} is assigned to C-H stretching vibration on unsaturated carbons (sp^2). Raman peak for CVD spectrum at 1360 cm^{-1} is attributed to disordered mode of graphite and that at 1500-1550 cm^{-1} corresponds to an amorphous-like structure with sp^3 and sp^2 bonding [61]. CVD-carbon layer has a broad peak at 1530 cm^{-1} indicating that the deposited layers are composed mostly of amorphous carbon with sp^3 and sp^2 bonds [68]. Peak at 1360 cm^{-1}, which is also present in evaporated and sputtered C-layers, is due to the presence of disordered graphite [68]. Band

position at 1617 cm^{-1} is typical for plane stretching C=C vibration (sp^2), called G ("graphite")-band in the case of carbon materials. From spectrum is obvious that layer deposited by evaporation and sputtering doesn't contain valence C-H vibration, which is normally appearing around 2950 cm^{-1}.

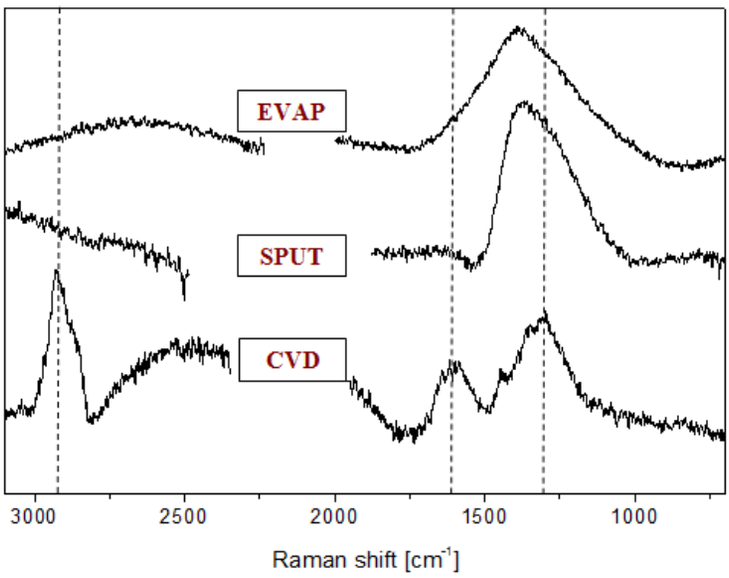

Figure 15. Raman spectra of pristine PET and carbon layers on PET prepared by evaporation, sputtering and CVD method. The layers have comparable thickness (approx. 80 nm).

Longer "structures" absorb on longer wave lengths. It was observed that in comparison with pristine PET the sputtered and CVD deposited C-layers are containing more conjugated double bonds. Dramatically an increase of amount of double bonds is present at the evaporated layers. This result is confirmed by measurement of sheet resistance. The sputtered and CVD layers show small decrease of R_s in comparison with pristine PET.

Significant decrease of 10 orders was measured for the evaporated C-layers. It was published that evaporated C-layers deposited by flash-evaporation were showing high electrical conductivity [41]. The concentrations of carbon, oxygen and nitrogen in the surface layer with the detection thickness around 1 μm were measured by RBS and ERDA After deposition of C-layers the increase of the carbon content was observed. The highest oxygen concentration being observed for sputtered C layers on PET.

2.6.4. Cells adhesion and proliferation

We have observed by the Raman spectroscopy, that there are no significant changes of the carbon layer after sterilization [39]. The sterilization in autoclave of the samples was performed 1 day before the experiment and then they were kept under sterile conditions. Adhesion and proliferation of 3T3 fibroblasts on the pristine PET and evaporated, sputtered and CVD coated foils with approximate C-layer thickness around 80 nm. The amount of adhered cells after 1 day of cultivation and proliferating cells after 3 and 5 days of cultivation is shown in Fig. 17. It is seen that the cells adhere similarly on all the surfaces

without any significant difference. The proliferation after 3 days is showing certain differences in the amount of the cells especially increase of the amount of the cells on the evaporated and sputtered layers.

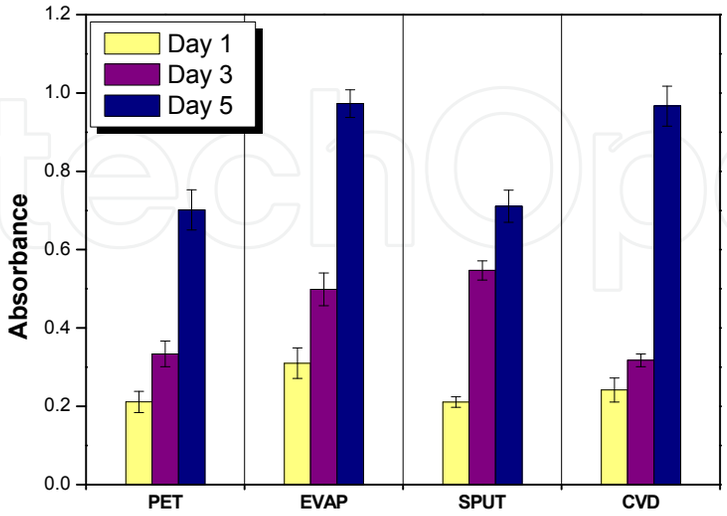

Figure 16. The amount of the 3T3 cells measured from absorbance of MTT test after adhesion (1st day) and proliferation (3rd and 5th day) on pristine PET and carbon layers on PET prepared by evaporation, sputtering and CVD method. The layers have comparable thickness (approx. 80 nm). The amount was calculated in respect to the tissue PS.

As was observed, the values of the water contact angle on the surface of evaporated and CVD deposited coatings are similar and slightly higher for sputtered layers. The amount of adhered cells after 24 hours is equal for all coatings, so there is no significant influence of the water contact angle (wetting properties) on the adhesion of the cells. The evaporated layers were showing high electrical conductivity in comparison with other techniques which is due to the creation of the conjugated systems of double bonds. An increase of electrical conductivity can be taken as the main factor positively influencing the proliferation of the 3T3 fibroblast cells on the evaporated surfaces compared to pristine PET.

3. Conclusions

The present results can be summarized as follows:

- carbon nanolayers for enhancing of surface biocompatibility can be prepared by sputtering, evaporation, CVD method or by nanoparticles deposition on polymer. The scheme in Fig. 19 represents the idea of our research,
- carbon layers deposited onto polymer substrate strongly influences the surface morphology, wettability and chemical structure of polymer's surface,
- PVD methods (sputtering, evaporation) and CVD deposition of carbon layers leads to the contact angle decrease and the surfaces wettability increase,
- carbon layer deposition leads to the significant decrease of surface sheet resistance,
- the sputtered carbon layers consist of amorphous hydrogenated carbon (a-C:H) containing an oxygen admixture,

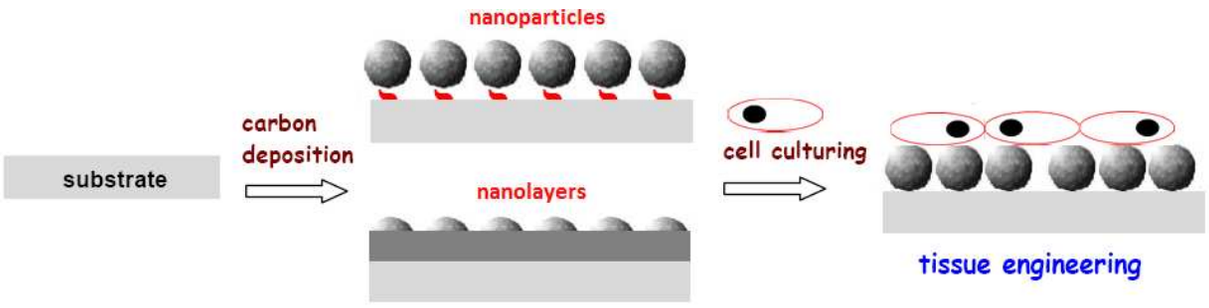

Figure 17. Vizualization of the individual steps of our research.

- the presence of sp^3 and sp^2 bonding declare the presence of double bonding system between the C atoms in case of CVD technique,
- surface morphology and carbon layer thickness is an important parameter influencing adhesion and short-term proliferation of cells,
- the chemical composition and surface wettability seems to be important parameter especially for long-term proliferation of the 3T3 fibroblasts,
- fullerenes C_{60} deposited as continuous films or layers micropatterned with grooves and bulges, Ti and C_{60}/Ti films used in this study gave good support to the adhesion, spreading, growth and viability of human osteoblast-like MG 63 cells,
- the large difference in cell adhesion and proliferation between pristine PTFE and carbon coated PTFE allows to confine the cells to certain areas at the surface, which opens a wide field of possible biomedical applications,
- carbon nanoparticle-containing materials supported adhesion and growth of bone-derived cells. The carbon nanoparticle layers, especially hard diamond coatings, could be used for surface modification of bone implants

Author details

Petr Slepička, Tomáš Hubáček, Simona Trostová,
Nikola Slepičková Kasálková and Václav Švorčík
Department of Solid State Engineering, Institute of Chemical Technology, Prague, Czech Republic

Zdeňka Kolská
Faculty of Science, J.E. Purkyně University, Ústí nad Labem, Czech Republic

Lucie Bačáková
Institute of Physiology, Academy of Sciences of the Czech Republic, Prague, Czech Republic

Acknowledgement

This work was supported by the GACR under projects P108/10/1106 and P108/12/1168.

4. References

[1] Chai F, Mathis N, Blanchemain N, Meunier C, Hildebrand HF (2008) Osteoblast Interaction with DLC-Coated Si Substrates. Acta biomater. 4: 1369-1381.

[2] Santavirta S (2003) Compatibility of the Totally Replaced Hip - Reduction of Wear by Amorphous Diamond Coating. Acta orthop. scand. suppl. 74: 310-316.

[3] Kobayashi S, Ohgoe Y, Ozeki K, Hirakuri K, Aoki H (2007) Dissolution Effect and Cytotoxicity of Diamond-Like Carbon Coatings on Orthodontic Archwires. J. mater. sci. mater. med. 18: 2263-2268.

[4] Roy RK, Lee KR (2007) Biomedical Applications of Diamond-Like Carbon Coatings: A Review. J. biomed. mater. res. B 83: 72-84.

[5] Schrand AM, Huang H, Carlson C, Schlager JJ, Osawa E, Hussain SM, Dai L (2007) Are Diamond Nanoparticles Cytotoxic? J. phys. chem. 111: 2-7.

[6] Bačáková L, Grausová L, Vandrovcová M, Vacík J, et al. (2008) In: Nanoparticles: New Research. Lombardi SL (Ed.). Hauppauge, New York: Nova Science Publishers, Inc. pp. 39-107.

[7] Amaral M, Dias AG, Gomes PS, Lopes MA, Silva RF (2008) Nanocrystalline Diamond: In Vitro Biocompatibility Assessment by MG63 and Human Bone Marrow Cells Cultures. J. biomater. res. A 87: 91-99.

[8] Gajewski W, Achatz P, Williams OA, Haenen K, Bustarret E, Stutzmann M, Garrido JA (2009) Electronic and Optical Properties of Boron-Doped Nanocrystalline Diamond Films. J. phys. rev. B 79: 045206.

[9] Nebel CE, Shin D, Rezek B, Tokuda N, Uetsuka H, Watanabe H (2007) Diamond and Biology. J. r. soc. interface 4: 439-461.

[10] Majid E, Male KB, Luong JHT (2008) Boron Doped Diamond Biosensor for Detection of Escherichia Coli. J. agric. food chem. 56: 7691-7695.

[11] Zhao J, Wu L, Zhi J (2009) Non-Enzymatic Glucose Detection Uusing As-Prepared Boron-Doped Diamond Thin-Film Electrodes. analyst 134: 794-799.

[12] Watari F, Takashi N, Yokoyama A, Uo M, Akasaka T, Sato Y, Abe S, Totsuka Y, Tohji K (2009) Material Nanosizing Effect on Living Organisms: Non-Specific, Biointeractive, Physical Size Effects. J. r. soc. interface 6: S371-S388.

[13] Aoki N, Akasaka T, Watari F, Yokoyama A (2007) Carbon Nanotubes as Scaffolds for Cell Culture and Effect on Cellular Functions. Dent. mater. j. 26: 178-185.

[14] Li X, Gao H, Uo M, Sato Y, Akasaka T, Abe S, Watari F (2009) Maturation of Osteoblast-Like SaoS2 Induced by Carbon Nanotubes. Biomed. mater. 4: 015005.

[15] Gonzalez KA, Wilson LJ, Wu W, Nancollas GH (2002) Synthesis and in Vitro Characterization of a Tissue-Selective Fullerene: Vectoring C-60(OH)(16)AMBP to Mineralized Bone. Bioorg. med. chem. 10: 1991-1997.

[16] Liu J, Tabata Y (2010) Photodynamic Therapy of Fullerene Modified with Pullulan on Hepatoma Cells. J. drug target. 18: 602-610.

[17] Marchesan S, Da Ros T, Spalluto G, Balzarini J, Prato M (2005) Anti-HIV Properties of Cationic Fullerene Derivatives. Bioorg. med. chem. lett. 15: 3615-3618.
[18] Huang LY, Terakawa M, Zhiyentayev T, Huang YY, Sawayama Y, Jahnke A, Tegos,GP, Wharton T, Hamblin MR (2010) Innovative Cationic Fullerenes as Broad-Spectrum Light-Activated Antimicrobials. Nanomedicine 6: 442-452.
[19] Dellinger A, Zhou Z, Lenk R, MacFarland D, Kepley CL (2009) Fullerene Nanomaterials Inhibit Phorbol Myristate Acetate-Induced Inflammation. Exp. dermatol. 18: 1079-1081.
[20] Maeda R, Noiri E, Isobe H, Homma T, Tanaka T, Nagishi K, Doi K, Fujita T, Nakamura E (2008) A Water-Soluble Fullerene Vesicle Alleviates Angiotensin II-Induced Oxidative Stress in Human Umbilical Venous Endothelial Cells. Hypertens. res. 31: 141-151.
[21] Tykhomyrov AA, Nedzvetsky VS, Klochkov VK, Andrievsky GV (2008) Nanostructures of Hydrated C-60 Fullerene (C(60)HyFn) Protect Rat Brain Against Alcohol Impact and Attenuate Behavioral Impairments of Alcoholized Animals. Toxicology 246: 158-165.
[22] Iijima S (2002) Carbon Nanotubes: Past, Present, and Future. Physica B 323: 1-5.
[23] Bačáková L, Grausová L, Vacík J, Fraczek A, Blazewicz S, Kromka A, Vaněček M, Švorčík V (2007) Improved Adhesion and Growth of Human Osteoblast-Like MG 63 Cells on Biomaterials Modified with Carbon Nanoparticles. Diamond relat. mater. 16: 2133-2140.
[24] Thostenson ET, Li C, Chou TW (2005) Nanocomposites in Context. Compos. sci. technol. 65: 491-516.
[25] Chester DW, Klemic JF, Stern E, Sigworth FJ, Klemic KG (2007) Holey Carbon Micro-Arrays for Transmission Electron Microscopy: A Microcontact Printing Approach. Ultramicroscopy 107: 685-691.
[26] Yubuta K, Hongo T, Atou T, Nakamura KG, Kikuchi M (2007) High-Resolution Electron Microscopy of Microstructure of MnF2 Subjected to Shock Compression at 4.4 GPa. Solid state commun. 143: 127-130.
[27] Sullivan JP, Friedman TA, Hjor K (2001) Diamond and Amorphous Carbon MEMS. MRS bull. 26: 309-311.
[28] Chiang KT, Yang L, Wei R, Coulter K (2008) Development of Diamond-Like Carbon-Coated Electrodes for Corrosion Sensor Applications at High Temperatures. Thin solid films 517: 1120-1124.
[29] Yang YL, Gupta MC, Dudley KL, Lawrence RW (2005) A Comparative Study of EMI Shielding Properties of Carbon Nanofiber and Multi-Walled Carbon Nanotube Filled Polymer Composites. J. nanosci. nanotechnol. 5: 927-931.
[30] Abbas GA, Roy SS, Papakonstantinou P, McLaughlin JA (2005) Structural Investigation and Gas Barrier Performance of Diamond-Like Carbon Based Films on Polymer Substrates. Carbon 43: 303-309.
[31] Bouvree A, Feller JF, Castro M, Grohens Y, Rinaudo M (2009) Conductive Polymer nano-bioComposites (CPC): Chitosan-Carbon Nanoparticle a Good Candidate to Design Polar Vapour Sensors. Sens. actuator B 138: 138-147.

[32] Masuda K, Ogawa M, Ohkita H, Benten H, Ito S (2009) Hybrid Solar Cells of Layer-by-Layer Thin Films with a Polymer/Fullerene Bulk Heterojunction. Sol. ener. mater. sol. cells 93: 762-767.
[33] Moniruzzaman M, Winey KI (2006) Polymer Nanocomposites Containing Carbon Nanotubes. Macromolecules 39: 5194-5205.
[34] Coleman JN, Khan U, Blau WJ, Gun'ko YK (2006) Small but Strong: A Review of the Mechanical Properties of Carbon Nanotube-Polymer Composites. Carbon 44: 1624-1652.
[35] Wang CC, Guo ZX, Fu S, Wu W, Zhu DB (2004) Polymers containing fullerene or carbon nanotube structures. Prog. polym. sci. 29: 1079-1141.
[36] Kuilla T, Bhadra S, Yao D, Kim NH, Bosed S, Lee JH (2010) Recent Advances in Graphene Based Polymer Composites. Prog. polym. sci. 35: 1350-1375.
[37] Švorčík V, Hubáček T, Slepička P, Siegel J, Kolská Z, Bláhová O, Macková A, Hnatowicz V (2009) Characterization of Carbon Nanolayers Flash Evaporated on PET and PTFE. Carbon 47: 1770-1778.
[38] Kubová O, Bačáková L, Švorčík V (2005) Biocompatibility of Carbon Layer on Polymer. Mater. sci. forum 482: 247-250.
[39] Kubová O, Švorčík V, Heitz J, Moritz S, Romanin C, Macková A (2007) Characterization and Cytocompatibility of Carbon Layers Prepared by Photo-Induced Chemical Vapor Deposition. Thin solid films 515: 6765-6772.
[40] Švorčík V, Kasálková N, Slepička P, Záruba K, Bačáková L, Pařízek M, Lisá V, Ruml T, Macková A (2009) Cytocompatibility of Ar(+) Plasma Treated and Au Nanoparticle-Grafted PE. Nucl. instrum. meth. B 267: 1904-1910.
[41] Hubáček T, Lyutakov O, Rybka V, Švorčík V (2010) Electrical Properties of Flash-Evaporated Carbon Nanolayers on PTFE. J. mater. sci. 45: 279-281.
[42] Stein A, Wang Z, Fierke MA (2009) Functionalization of Porous Carbon Materials with Designed Pore Architecture. Adv. mater. 21: 265-293.
[43] Narayan RJ (2005) Nanostructured Diamond-Like Carbon Thin Films for Medical Applications. Mater. sci. eng. 25: 405-416.
[44] Wang DY, Chang YY, Chang CL, Huang YW (2005) Deposition of Diamond-Like Carbon Films Containing Metal Elements on Biomedical Ti Alloys. Surf. coat. technol. 200: 2175-2180.
[45] Švorčík V, Kubová O, Slepička P, Dvořánková B, Macková A, Hnatowicz V (2006) Structural, Chemical and Biological Properties of Carbon Layers Sputtered on PET. J. mater. sci. mater. med.17: 229-234.
[46] Zhang L, Webster TJ (2009) Nanotechnology and Nanomaterials: Promises for Improved Tissue Regeneration. Nano today 4: 66-80.
[47] Kim S, Shibata E, Sergiienko R, Nakamura T (2008) Purification and Separation of Carbon Nanocapsules as a Magnetic Carrier for Drug Delivery Systems. Carbon 46: 1523-1529.
[48] Schroeder A, Francz G, Bruinink A, Hauert R, Mayer J, Wintermantel E (2000) Titanium Containing Amorphous Hydrogenated Carbon Films (a-C: H/Ti): Surface Analysis and

Evaluation of Cellular Reactions Using Bone Marrow Cell Cultures in Vitro. Biomaterials 21: 449-456.

[49] Ma WJ, Ruys AJ, Mason RS, Martin PJ, Bendavid A, Liu Z, Ionescu M, Zreiqat H (2007) DLC Coatings: Effects of Physical and Chemical Properties on Biological Response. Biomaterials 28: 1620-1628.

[50] Greer JA, Tabat MD (1995) Large-Area Pulsed Laser Deposition: Technique and Application. J. vac. sci. technol. A 13: 1175-1181.

[51] McLaughlin JA, Maguire PD (2008) Advances on the Use of Carbon Materials at the Biological and Surface Interface for Applications in Medical Implants. Diam. relat. mater. 17: 873-877.

[52] Kotál V, Švorčík V, Slepička P, Bláhová O, Šutta P, Hnatowicz V (2007) Gold Coating of PET Modified by Argon Plasma. Plasma proc. polym. 4: 69-76.

[53] Pradhan D, Sharon M (2007) Opto-Electrical Properties of Amorphous Carbon Thin Film Deposited from Natural Precursor Camphor. Appl. surf. sci. 253: 7004-7010.

[54] Mott N (1990) Metal Insulator Transitions. London: Taylor & Francis. p.1-286.

[55] Švorčík V, Kolská Z, Luxbacher T, Mistrík J (2010) Properties of Au Nanolayer Sputtered on Polyethyleneterephthalate. Mater. lett. 64: 611-613.

[56] Avigal Y, Kalish R (2001) Growth of Aligned Carbon Nanotubes by Biasing During Growth. Appl. phys. lett. 78: 2291-2293.

[57] Cappelli E, Orlando S, Mattei G, Zoffoli S, Ascarelli P (2002) SEM and Raman Investigation of RF Plasma Assisted Pulsed Laser Deposited Carbon Films. Appl. surf. sci. 197-198: 452-457.

[58] Švorčík V, Ročková K, Dvořánková B, Hnatowicz V, Ochsner R, Ryssel H (2002) Cell Adhesion on Modified Polyethylene. J. Mater. Sci. 37: 1183-1188.

[59] Yang P, Kwok SCH, Fu RKY, Huang N, Leng Y, Chu PK (2004) Structure and properties of Annealed Amorphous Hydrogenated Carbon (a-C : H) Films for Biomedical Applications. Surf. coat. technol. 177: 747-751.

[60] Levi N, Hantgan RR, Lively MO, Carroll DL, Prasad GL (2006) C60-Fullerenes: detection of intracellular photoluminescence and lack of cytotoxic effects. J. nanobiotechnol. 4: 14.

[61] Nakamura E, Isobe H (2003) Functionalized Fullerenes in Water. The First 10 Years of Their Chemistry, Biology, and Nanoscience. Acc. chem. res. 36: 807-815.

[62] Grausová L, Vacík J, Švorčík V, Slepička P, Bílková P, Vandrovcová M, Lisá V, Bačáková L (2009) Fullerene C(60) Films of Continuous and Micropatterned Morphology as Substrates for Adhesion and Growth of Bone Cells. Diamond rel. mater. 18: 578-586.

[63] Vandrovcová M, Vacík J, Švorčík V, Slepička P, Kasálková N, Vorlíček V, Lavrentiev V, Voseček V, Grausová L, Lisá V, Bačáková L (2008) Fullerene C-60 and Hybrid C-60/Ti Films as Substrates for Adhesion and Growth of Bone Cells. Phys. stat. sol. A 205: 2252-2261.

[64] Endo M, Hayashi T, Kim YA, Terrones M, Dresselhaus MS (2004) Applications of Carbon Nanotubes in the Twenty-First Century. Philos. transact. r. soc. A math. phys. eng. sci. 362: 2223-2238.
[65] Kohli P, Martin CR (2005) Smart Nanotubes for Biotechnology. Curr. pharm. biotechnol. 6: 35-47.
[66] Bačáková L, Starý V, Kofroňová O, Lisá V (2001) Polishing and Coating Carbon Fiber-Reinforced Carbon Composites with a Carbon-Titanium Layer Enhances Adhesion and Growth of Osteoblast-Like MG63 Cells and Vascular Smooth Muscle Cells in Vitro. J. biomed. mater. res. 54: 567-578.
[67] Švorčík V, Kolářová K, Slepička P, Macková A, Novotná M, Hnatowicz V (2006) Modification of Surface Properties of High and Low Density Polyethylene by Ar Plasma Discharge. Polym. degr. stab. 91: 1219-1225.
[68] Li DJ, Cui FZ, Gu HQ (1999) Studies of Diamond-Like Carbon Films Coated on PMMA by Ion Beam Assisted Deposition. Appl. surf. sci. 137: 30-37.

IntechOpen